

Model-Based Vector-Fitting Method for Circuit Model Extraction of Coupled-Resonator Diplexers

Ping Zhao, *Student Member, IEEE*, and Ke-Li Wu, *Fellow, IEEE*

Abstract—In this paper, a novel rational function approximation method, namely, model-based vector fitting (MVF), is proposed for accurate extraction of the characteristic functions of a coupled-resonator diplexer with a resonant type of junction from noise-contaminated measurement data. MVF inherits all the merits of the vector-fitting (VF) method and can also stipulate the order of the numerator of the model. Thus, MVF is suitable for the high-order diplexer system identification problem against measurement noise. With the extracted characteristic functions, a three-port transversal coupling matrix of a diplexer can be synthesized. A matrix orthogonal transformation strategy is also proposed to transform the obtained transversal matrix to a target coupling matrix configuration, whose entries have one-to-one relationship with the physical tuning elements. The whole model extraction procedure is analytical and robust, and can be used in a computer-aided tuning (CAT) program for coupled-resonator diplexers. A practical tuning example of a diplexer with a common resonator is given in detail to demonstrate the effectiveness and the practical value of the proposed method.

Index Terms—Computer-aided tuning (CAT), coupling matrix, microwave diplexer, rational approximation, vector fitting (VF).

I. INTRODUCTION

COUPLED resonator networks are commonly utilized as frequency-selective devices in RF and microwave passive circuits such as filters, diplexers, and multiplexers, and play very important roles in modern communication systems. It is well known that the transfer and reflection characteristics of a coupled-resonator network can be described by a set of rational functions [1]. The concept has been successfully applied not only to the design of bandpass filters, but also other functional microwave networks such as power dividers [2], diplexers [3], multiple-input multiple-output (MIMO) antenna decoupling networks [4], and nonreciprocal networks [5]. There are various ways to implement a coupled-resonator network: coupled waveguide resonant cavities, coupled coaxial combine resonators, and coupled dielectric resonators of multiple modes are commonly seen in today's communication systems.

Manuscript received October 16, 2015; revised March 31, 2016; accepted April 21, 2016. Date of publication May 9, 2016; date of current version June 2, 2016. This work was supported by The Chinese University of Hong Kong under a Postgraduate Scholarship. This work was supported in part by the Development and Reform Commission of Shenzhen Municipality under Grant Shen Fa Gai (2013) 1673.

The authors are with the Department of Electronic Engineering and the Shenzhen Engineering Laboratory of Wireless Locating Technology and Systems, Shenzhen Research Institute, The Chinese University of Hong Kong, Shatin, Hong Kong (e-mail: pzhao@ee.cuhk.edu.hk; kluwu@ee.cuhk.edu.hk).

Color versions of one or more of the figures in this paper are available online at <http://ieeexplore.ieee.org>.

Digital Object Identifier 10.1109/TMTT.2016.2558639

In mass production of such microwave devices, the physical realization is highly sensitive to the dimensional tolerance of the resonators as well as the coupling elements. Therefore, manual tuning is necessary in the production process to meet the stringent system specifications. Traditionally, the tuning is accomplished by skilled technologists through consecutive manual adjustments based on their years of accumulated experience. Tuning a coupled-resonator device with a complex coupling topology is a demanding, time-consuming, and costly process. A computer-aided tuning (CAT) tool that can identify those unsatisfying coupling values and deterministically guide the tuning process is highly appreciated in the microwave industry. With such a CAT tool, the tuning process will depend much less on human experience and the cost of the production can be greatly reduced.

Up to now the majority of research efforts devoted to CAT algorithms are for bandpass filters [6]–[11]. With the measured (or electromagnetic (EM) simulation) results of the device, the circuit model that corresponds to the current tuning state is extracted, which is then compared with the designed circuit model to suggest the tuning direction and amount for the next tuning step.

Obviously, the most critical and difficult part in the CAT procedure is the extraction of the circuit model from measured data. Although this task can be undertaken by optimization techniques [7], such approaches are time consuming and heavily depend on a set of good initial values. It is much more difficult to analytically extract the circuit model of a diplexer than that of a filter for three major reasons. First, the interaction between the two channel filters makes the diplexer a high-order system. The traditional rational function approximation method, like the Cauchy method, has the problem of ill conditioning when it is used to deal with high-order systems. Second, to meet the stringent requirement of Tx and Rx isolation, complex coupling topologies are commonly seen in a diplexer introducing finite-position transmission zeroes (TZs) to improve the isolation. As a result, how to obtain the circuit model, which can give the identical response with the device and has the same coupling structure, is a challenging problem. Third, the measured frequency response of the diplexer is inevitably contaminated by measurement noise, and the isolation characteristics can be completely buried by the noise floor. Although there are some discussions on diplexer circuit model extraction in the literature [12], no practical application has yet been presented.

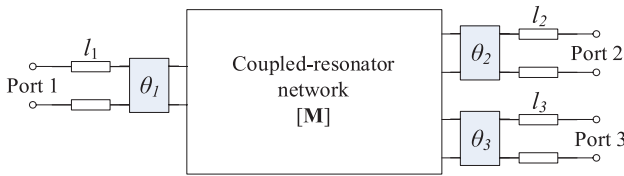


Fig. 1. Complete circuit model that corresponds to practical measurement or EM simulation of a general three-port coupled-resonator network.

To address the mentioned issues, a new rational function approximation method called the model-based vector fitting (MVF) is proposed in [13]. This paper is a substantial extension of [13] where several issues related to the implementation of MVF, including the selection of initial poles and the iterative pole relocation procedure, are further elaborated upon in this paper. Additionally, the details of how to synthesize the three-port transversal coupling matrix from the obtained rational functions are explained. A novel similarity transformation strategy is also proposed in this paper, which reconfigures the transversal coupling matrix to the right matrix configuration. The strategy can be generalized to be suitable for other star-junction diplexers with common resonant nodes.

The basic theory on the multi-port coupled-resonator network underlying the circuit model extraction method is briefly introduced first. The MVF method is then proposed for fitting the characteristic functions of the coupled-resonator diplexer, which evolves from the original vector-fitting (VF) technique and solves the “over-fitting” and “under-fitting” problems with the VF approach. By introducing a set of *pole-located monomials* as the basis functions, MVF enjoys the merits of the traditional Cauchy method, by which the order of the numerator of a rational function can be stipulated in the fitting procedure and the VF method, by which the conditioning of the system equations is better and the accuracy of the fitting is improved by the iterative pole relocation procedure. How a three-port transversal coupling matrix is synthesized from the poles and residues determined in MVF is described, and then the transversal matrix is reconfigured to the right form following a sequence of similarity transformations. The measured data of several tuning states of a coupled-resonator diplexer with a common resonator are used to illustrate the complete circuit model extraction procedure. It can be seen that the extracted circuit model with the method proposed in this paper can capture very subtle adjustment made to the physical tuning elements, which validates the robustness and the practical value of the proposed method.

II. ADMITTANCE MATRIX OF A COUPLED RESONATOR DIPLEXER

A. De-Embedding of the Phase Offset

For any practical measurement or EM simulation setup of a coupled-resonator diplexer, the proper circuit model that can represent the entire system is depicted in Fig. 1. As discovered in [9], there is a constant phase loading θ_x that results from the high-order modes associated with I/O coupling at each port. Besides, a piece of transmission line l_x is there for

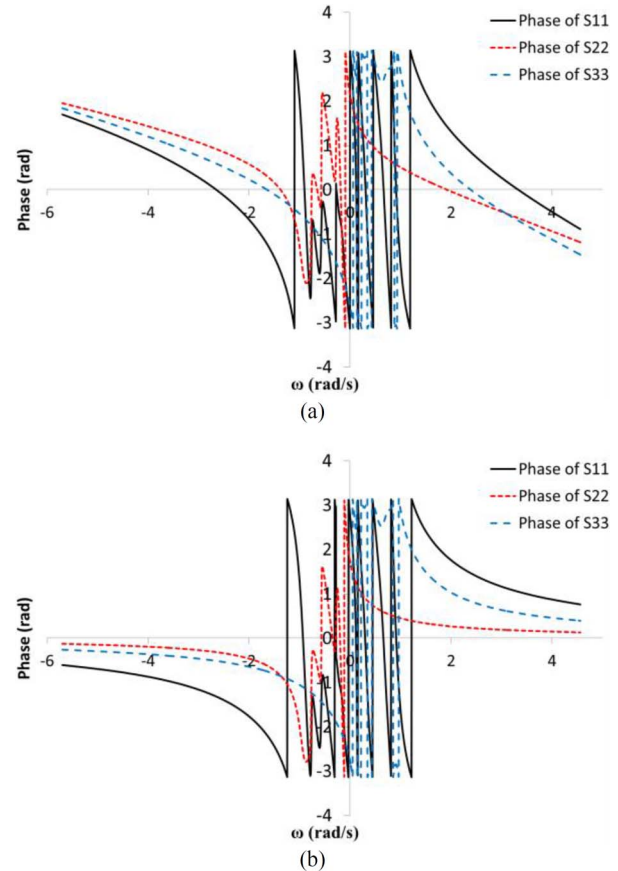


Fig. 2. (a) Phases of S_{11} , S_{22} , and S_{33} of the raw measured data. (b) Phases of S_{11} , S_{22} , and S_{33} after removing the phase loading and de-embedding the transmission line at each port.

connection of the device in practical measurement setup, or for extending and clearly defining the port in EM simulation. The center block of Fig. 1 is the body of the diplexer composed of coupled resonators, which can be described by a three-port coupling matrix \mathbf{M} . In [9], the phase loading effect and the transmission line are removed by observing the asymptotic phase response of each reflection coefficient beyond the passband. For example, Fig. 2(a) shows the phases of the measured reflection coefficients from one of the tuning states of the testing diplexer shown in Fig. 3(a) with respect to the normalized low-pass domain angular frequency variable, and Fig. 2(b) shows the phases after phase loading and transmission lines are de-embedded, where the phases of the reflection coefficients approach zero as s approaches infinity. Correct removal of the phase offset is crucial for identifying the true poles and zeroes of the Y -parameters.

B. Multi-Port Coupling Matrix

After the phase offset at each port is de-embedded, the S -parameters are then converted to Y -parameters numerically with respect to unitary reference admittance at all ports. The Y -parameters are then consistent with the short-circuit admittance characteristics of a coupled-resonator circuit model with J -inverters as the leading elements at all port. A multi-port coupled-resonator network can be described by a coupling

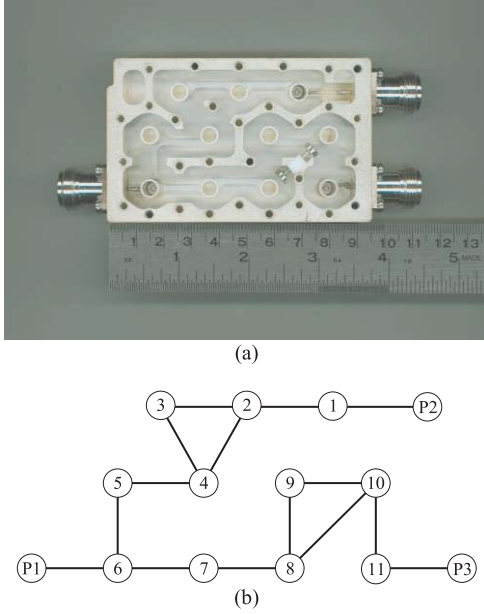


Fig. 3. (a) Photograph of the testing diplexer. (b) Routing diagram of the testing diplexer. Circles marked P1–P3 represent the three ports and the other circles represent resonators. Solid straight lines are either mutual couplings between resonators or I/O couplings.

matrix in the form of block matrices as

$$\mathbf{M} = \begin{bmatrix} \mathbf{M}_p & \mathbf{M}_{pn} \\ \mathbf{M}_{pn}^T & \mathbf{M}_n \end{bmatrix} \quad (1)$$

where \mathbf{M}_p is a p -by- p sub-matrix consisting of direct couplings between the p ports, \mathbf{M}_n is an n -by- n sub-matrix containing all the mutual couplings between the n resonators and the self-couplings of resonators, \mathbf{M}_{pn} is a p -by- n sub-matrix holding all the I/O couplings, and superscript T denotes the matrix transpose. The relationship between the Y -parameters and \mathbf{M} is found to be [14]

$$\begin{aligned} \mathbf{Y} &= j\mathbf{M}_p + \mathbf{M}_{pn}(s\mathbf{I}_n + j\mathbf{M}_n)^{-1}\mathbf{M}_{pn}^T \\ &= j\mathbf{M}_p + \sum_{k=1}^n \frac{1}{s + j\mathbf{M}_n(k, k)} \mathbf{M}_{pn}(:, k) \mathbf{M}_{pn}(:, k)^T \end{aligned} \quad (2)$$

where $\mathbf{M}_{pn}(:, k)$ denotes the k th column vector in the matrix \mathbf{M}_{pn} . From (2), two basic properties can be observed: 1) the elements in the Y -parameters share a set of common poles and 2) the residue matrix is symmetric and is of rank one. The second property is called the *compactness* of the residues.

To correctly restore the coupling matrix of a diplexer, the above-mentioned two properties must be satisfied by the Y -parameter rational functions. The first property can be enforced during the rational fitting procedure, as will be demonstrated in Section III. The second condition will not be implemented since otherwise quadratic constraints are involved and nonlinear optimization techniques are needed to solve the problem. However, in applying the MVF technique to the measured data of a physical coupled-resonator network, the residues obtained by the rational function approximation procedure to be discussed next always well satisfy the second

property with very small numerical errors, provided that the phase offset at each port has been correctly de-embedded. Thus, a transversal coupling matrix can still be synthesized, which will be discussed in Section IV.

III. MVF FORMULATION

To explain the circuit model extraction procedure, measured data of the coaxial resonator diplexer shown in Fig. 3(a) are used. The diplexer is introduced in [15], whose lower frequency band is 2.478–2.568 GHz, and upper frequency band is 2.620–2.718 GHz. The routing diagram of the diplexer is shown in Fig. 3(b), where hollow circles with numbers inside represent resonators and the solid straight lines represent couplings. The two channel filters both consist of five resonators, and resonator No. 6 constitutes a resonant type of junction.

Once the measured data are obtained, the physical frequency is mapped to the low-pass frequency domain by

$$\omega = \frac{f_0}{\text{BW}} \left(\frac{f}{f_0} - \frac{f_0}{f} \right) \quad (3)$$

where, in this case, $f_0 = \sqrt{2.478 \times 2.718} = 2.595$ GHz, and $\text{BW} = 2.718 - 2.478 = 0.24$ GHz, respectively. The complex frequency variable $s = j\omega$ will be used in the rational function description of the characteristic functions.

The phase offset at each port is first de-embedded from the measured S -parameters, as mentioned in Section II-A. The S -parameters are then converted to Y -parameters for identifying the poles and residues in order to obtain the transversal coupling matrix for the diplexer.

A. Original VF

A method of finding the rational function approximation can find applications in many engineering fields. A milestone in the history of solving the rational function approximation problem is the development of the VF technique [16], [17]. VF outperforms the Cauchy formulation in that it adopts *partial fractions* as the basis functions instead of the *monomials*, thus rectifies the ill-conditioning problem and substantially improves the robustness of the system equations. In the diplexer circuit model extraction problem, there are six rational functions to be determined, i.e., Y_{11} , Y_{12} , Y_{13} , Y_{22} , Y_{23} , and Y_{33} in the three-port reciprocal Y -matrix of a diplexer. Using the VF approach, to ensure all the rational functions share the same poles, the system equations are assembled in the form of block matrices as

$$\begin{bmatrix} \mathbf{A}_1 & \mathbf{0} & \mathbf{0} & \mathbf{0} & \mathbf{0} & \mathbf{0} & -\mathbf{Y}_{11}\mathbf{A}_2 \\ \mathbf{0} & \mathbf{A}_1 & \mathbf{0} & \mathbf{0} & \mathbf{0} & \mathbf{0} & -\mathbf{Y}_{12}\mathbf{A}_2 \\ \mathbf{0} & \mathbf{0} & \mathbf{A}_1 & \mathbf{0} & \mathbf{0} & \mathbf{0} & -\mathbf{Y}_{13}\mathbf{A}_2 \\ \mathbf{0} & \mathbf{0} & \mathbf{0} & \mathbf{A}_1 & \mathbf{0} & \mathbf{0} & -\mathbf{Y}_{22}\mathbf{A}_2 \\ \mathbf{0} & \mathbf{0} & \mathbf{0} & \mathbf{0} & \mathbf{A}_1 & \mathbf{0} & -\mathbf{Y}_{23}\mathbf{A}_2 \\ \mathbf{0} & \mathbf{0} & \mathbf{0} & \mathbf{0} & \mathbf{0} & \mathbf{A}_1 & -\mathbf{Y}_{33}\mathbf{A}_2 \end{bmatrix} \begin{bmatrix} \mathbf{c}_{11} \\ \mathbf{c}_{12} \\ \mathbf{c}_{13} \\ \mathbf{c}_{22} \\ \mathbf{c}_{23} \\ \mathbf{c}_{33} \\ \tilde{\mathbf{c}} \end{bmatrix} = \begin{bmatrix} \mathbf{y}_{11} \\ \mathbf{y}_{12} \\ \mathbf{y}_{13} \\ \mathbf{y}_{22} \\ \mathbf{y}_{23} \\ \mathbf{y}_{33} \end{bmatrix} \quad (4)$$

where

$$\text{the } i\text{th row of } \mathbf{A}_1 = \begin{bmatrix} 1 & 1 & \dots & 1 \\ s_i - a_1 & s_i - a_2 & \dots & s_i - a_N \end{bmatrix} \quad (5a)$$

$$\mathbf{A}_1 \in \mathbb{C}^{m \times (N+1)}$$

$$\text{the } i\text{th row of } \mathbf{A}_2 = \begin{bmatrix} 1 & 1 & \dots & 1 \\ s_i - a_1 & s_i - a_2 & \dots & s_i - a_N \end{bmatrix} \quad (5b)$$

$$\mathbf{A}_2 \in \mathbb{C}^{m \times N}$$

$$\mathbf{Y}_{pq} = \text{diag}\{Y_{pq}(s_i)\} \in \mathbb{C}^{m \times m} \quad (5c)$$

$$\mathbf{y}_{pq} = [Y_{pq}(s_1) \dots Y_{pq}(s_m)]^T \in \mathbb{C}^{m \times 1} \quad (5d)$$

$$\mathbf{c}_{pq} = [c_1^{pq} \ c_2^{pq} \ \dots \ c_N^{pq} \ d^{pq}]^T \in \mathbb{C}^{(N+1) \times 1} \quad (5e)$$

$$\tilde{\mathbf{c}} = [\tilde{c}_1 \ \tilde{c}_2 \ \dots \ \tilde{c}_N]^T \in \mathbb{C}^{N \times 1}. \quad (5f)$$

In (5a) and (5b), a_k is the k th pole of the system equations. In (5e) and (5f), c_k^{pq} is the residue corresponding to a_k and d^{pq} is the constant term of the numerator rational function of Y_{pq} . \tilde{c}_k is the residue of the denominator rational function. m is the number of sampling points and N is the order of the system. For the diplexer shown in Fig. 3, $N = 11$ because there are a total of 11 resonators. It can be seen from (5a) and (5b) that the VF formulation uniformly adopts partial fractions as the basis functions to fit all six of the Y -parameters.

After the residues \mathbf{c}_{pq} and $\tilde{\mathbf{c}}$ are obtained by solving (4) in the sense of least squares (LSs), the new system poles are located to the zeroes of

$$\sum_{k=1}^N \frac{\tilde{c}_k}{s - a_k} + 1 = 0 \quad (6)$$

which is known as the *iterative pole relocation* process of VF. Direct computation of the roots of the high-order numerator polynomial of (6) can be inaccurate. Alternatively, they can be accurately and conveniently calculated as the eigenvalues of the matrix [16]

$$\mathbf{A} - \mathbf{b} \cdot \tilde{\mathbf{c}}^T \quad (7)$$

where \mathbf{A} is an N -by- N diagonal matrix holding the original poles a_k . \mathbf{b} is a column vector of ones and its dimension is N . $\tilde{\mathbf{c}}$ is defined by (5f) and superscript T denotes the matrix transpose.

The system (4) are then updated with the newly computed poles a_k and are solved in an iterative manner until convergence is achieved. Convergence of the iterative pole relocation procedure is achieved when the elements of the vector $\tilde{\mathbf{c}}$ become sufficiently close to zero. The procedure converges fast, normally within a few iterations, and it is not sensitive to the choice of the initial set of poles a_k .

For general applications the starting poles are suggested to be chosen as complex numbers with small negative real parts, and their imaginary parts covering the frequency interval of interest, to avoid the ill-conditioning problem of the system matrix [17]. In the system identification problem of the testing diplexer, the 11 initial poles are chosen as

$$\begin{aligned} & -0.01 - 1j, -0.0079 - 0.79j, -0.0058 - 0.58j \\ & -0.0037 - 0.37j - 0.0016 - 0.16j, -0.0005 + 0.05j \\ & \quad - 0.0026 + 0.26j - 0.0047 + 0.47j \\ & -0.0068 + 0.68j, -0.0089 + 0.89j, -0.011 + 1.1j \end{aligned}$$

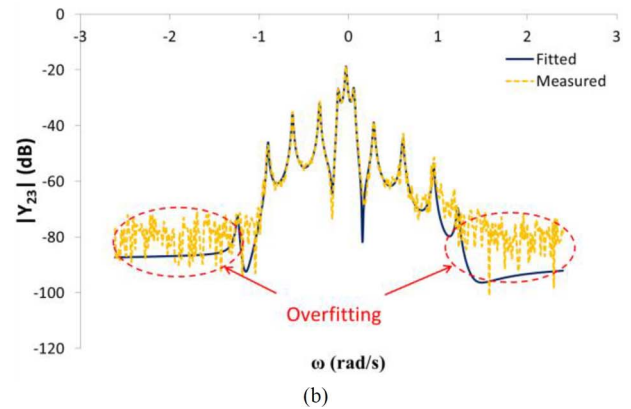
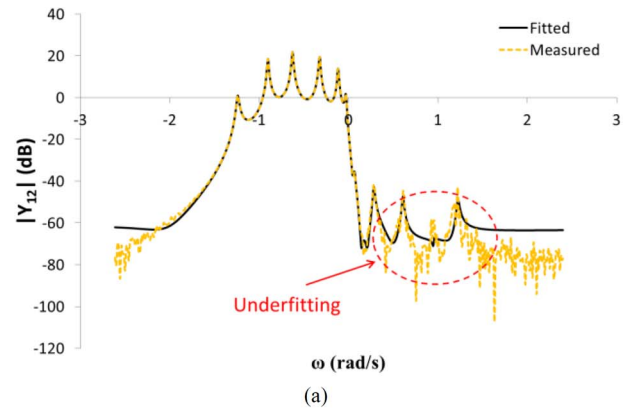


Fig. 4. (a) Measured and fitted data of Y_{12} with the VF approach. (b) Measured and fitted data of Y_{23} . Dash lines are the Y -parameter converted from the measured S -parameter with phase offset removed. Solid lines represent the rational approximation result given by VF.

where the imaginary parts are linearly distributed in $[-1, 1.1]$ and the real parts are all negative and the values are 1% of those of the imaginary parts.

The comparison between the measured and the fitted Y_{12} and Y_{23} are shown in Fig. 4(a) and (b) in a logarithmic scale. Two issues are identified in the fitting results. The first one is that the trans-admittances Y_{12} is *under-fitted* outside of the passband, where those data with small magnitude are not well fitted. Another issue is the *over-fitting* problem in Y_{23} fitting, where the model is trying to fit the measurement noise, whereas the true response is obviously buried by measurement noise beyond the passband.

B. MVF Formulation

In order to deal with the “under-fitting” and “over-fitting” problems in the original VF formulation for diplexer system identification, the MVF formulation is proposed, which introduces the *pole-located monomials* as the basis functions and includes proper weighting factors to improve the accuracy of the fitting result.

As the system is solved in the sense of LS, which aims at minimizing the sum of the squares of absolute errors, those data with large absolute values will dominate in the procedure, leading to absolutely small, but relatively large, fitting errors for those small data, which also contain important information

of the current state of the coupled resonators. In order to stress the significance of those small-valued data, the weighting factors, chosen as

$$W_{pq} = \frac{1}{\sqrt{|Y_{pq}|}} \quad (8)$$

are multiplied to the data of Y_{12} and Y_{13} , which magnify the LS error of small data and minify the error of large data, thus the relative accuracy can be balanced. However, at the same time, when the LS error of small data is stressed, the measurement noise is also magnified, which deteriorates the “over-fitting” problem.

It is well known that, for a coupled-resonator filter, both the order of the numerator of the transfer function S_{12} and that of the trans-admittance Y_{12} are equal to the number of TZs, which can be told from the routing diagram of the resonators. It is the same with a coupled-resonator diplexer network. For example, in the testing diplexer, there is a tri-section in each channel filter that introduces one TZ, and the five resonators from the other channel filter contribute five additional complex TZs on the left half s -plane. Thus, both orders of the numerators of Y_{12} and Y_{13} are 6. The order of the numerator of Y_{23} is 2 as a result of the two cascaded tri-sections. Taking the parasitic couplings into consideration, a more practical estimation is that the orders of the numerators of Y_{12} , Y_{13} , and Y_{23} are 7, 7, and 4, respectively.

The original VF formulation (4) uniformly adopts the *partial fractions* as the basis functions for all six of the Y -parameters in the Y -matrix. The model of linear combination of partial fractions gives the numerator an excessive degree of freedom than that actually needed, which makes the model over attempting to fit the measurement noise in the fitting of the trans-admittances. Thus, the VF approach leads to the “over-fitting” problem. In other words, the order of the numerator cannot be fixed to be a number less than $N - 1$ in the following equation:

$$Y_{pq}(s_i) \simeq \frac{p(s_i)}{\sigma(s_i)} = \frac{\left(\sum_{k=1}^N \frac{c_k^{ij}}{s_i - a_k} \right) + d^{ij}}{\left(\sum_{k=1}^N \frac{\tilde{c}_k^{ij}}{s_i - a_k} \right) + 1}, \quad i = 1, 2, \dots, m \quad (9)$$

where m denotes the total number of sampled data.

To rectify this problem, for the self-admittance functions Y_{11} , Y_{22} , and Y_{33} , whose numerators and denominators are of the same order (if the diagonal elements of $j\mathbf{M}_p$ in (2) are allowed to be non-zero), *partial fractions* are adopted as the basis functions. For the trans-admittance functions Y_{12} , Y_{13} , and Y_{23} , a new set of basis functions called *pole-located monomials* defined by

$$\frac{1}{\prod_{k=1}^N (s - a_k)}, \frac{s}{\prod_{k=1}^N (s - a_k)}, \dots, \frac{s^{Nz}}{\prod_{k=1}^N (s - a_k)} \quad (10)$$

are adopted, where Nz is the stipulated order of the numerator. Combining the weighting factors in (8) and replacing the partial fraction basis functions for trans-admittance by the

new pole-located monomial basis functions in (10), (4) can be reformulated as

$$\begin{bmatrix} \mathbf{A}_1 & \mathbf{0} & \mathbf{0} & \mathbf{0} & \mathbf{0} & \mathbf{0} & -\mathbf{Y}_{11}\mathbf{A}_2 \\ \mathbf{0} & \mathbf{W}_{12}\mathbf{A}_3 & \mathbf{0} & \mathbf{0} & \mathbf{0} & \mathbf{0} & -\mathbf{W}_{12}\mathbf{Y}_{12}\mathbf{A}_2 \\ \mathbf{0} & \mathbf{0} & \mathbf{W}_{13}\mathbf{A}_3 & \mathbf{0} & \mathbf{0} & \mathbf{0} & -\mathbf{W}_{13}\mathbf{Y}_{13}\mathbf{A}_2 \\ \mathbf{0} & \mathbf{0} & \mathbf{0} & \mathbf{A}_1 & \mathbf{0} & \mathbf{0} & -\mathbf{Y}_{22}\mathbf{A}_2 \\ \mathbf{0} & \mathbf{0} & \mathbf{0} & \mathbf{0} & \mathbf{A}_4 & \mathbf{0} & -\mathbf{Y}_{23}\mathbf{A}_2 \\ \mathbf{0} & \mathbf{0} & \mathbf{0} & \mathbf{0} & \mathbf{0} & \mathbf{A}_1 & -\mathbf{Y}_{33}\mathbf{A}_2 \end{bmatrix} \begin{bmatrix} \mathbf{c}_{11} \\ \mathbf{c}_{12} \\ \mathbf{c}_{13} \\ \mathbf{c}_{22} \\ \mathbf{c}_{23} \\ \mathbf{c}_{33} \\ \tilde{\mathbf{c}} \end{bmatrix} = \begin{bmatrix} \mathbf{y}_{11} \\ \mathbf{W}_{12}\mathbf{y}_{12} \\ \mathbf{W}_{13}\mathbf{y}_{13} \\ \mathbf{y}_{22} \\ \mathbf{y}_{23} \\ \mathbf{y}_{33} \end{bmatrix} \quad (11)$$

where

$$\mathbf{W}_{12} = \text{diag}\left\{ \frac{1}{\sqrt{|Y_{12}(s_i)|}} \right\} \in \mathbb{R}^{m \times m} \quad (12a)$$

$$\mathbf{W}_{13} = \text{diag}\left\{ \frac{1}{\sqrt{|Y_{13}(s_i)|}} \right\} \in \mathbb{R}^{m \times m} \quad (12b)$$

the i th row of \mathbf{A}_3

$$= \left[\frac{1}{\prod_{k=1}^N (s_i - a_k)} \frac{s_i}{\prod_{k=1}^N (s_i - a_k)} \dots \frac{s_i^7}{\prod_{k=1}^N (s_i - a_k)} \right] \quad (12c)$$

$\mathbf{A}_3 \in \mathbb{C}^{m \times 8}$

the i th row of \mathbf{A}_4

$$= \left[\frac{1}{\prod_{k=1}^N (s_i - a_k)} \frac{s_i}{\prod_{k=1}^N (s_i - a_k)} \dots \frac{s_i^4}{\prod_{k=1}^N (s_i - a_k)} \right] \quad (12d)$$

$\mathbf{A}_4 \in \mathbb{C}^{m \times 5}$.

Different from the variables in (4), with the pole-located monomials as the basis functions for Y_{12} , Y_{13} , and Y_{23} , the variables $\mathbf{c}_{12} \in \mathbb{C}^{8 \times 1}$, $\mathbf{c}_{13} \in \mathbb{C}^{8 \times 1}$, and $\mathbf{c}_{23} \in \mathbb{C}^{5 \times 1}$ in (11) are not the residues. In stead they are the coefficients of the basis functions defined by (10).

With the new basis functions, the *iterative pole relocation* procedure of the original VF formulation are retained to guarantee the accuracy of the poles and residues obtained. The initial poles are chosen as the same with those in previous VF formulation and convergence is also achieved within a few iterations.

For comparison purposes, the fitting of Y_{12} and Y_{23} using the MVF approach are shown in Fig. 5(a) and (b), respectively. The improvement is obvious as compared with Fig. 4(a) and (b) in that those small data in Y_{12} and Y_{13} are better fitted in the presence of measurement noise and Y_{23} is accurately recovered under the noise floor.

The MVF adopts mixed basis functions to fit the elements in the Y -matrix together. In the new formulation, the orders of the numerators are stipulated to be consistent with the coupling topology of the diplexer. Thus it can reduce the model's sensitivity to the measurement noise in a practical measurement environment.

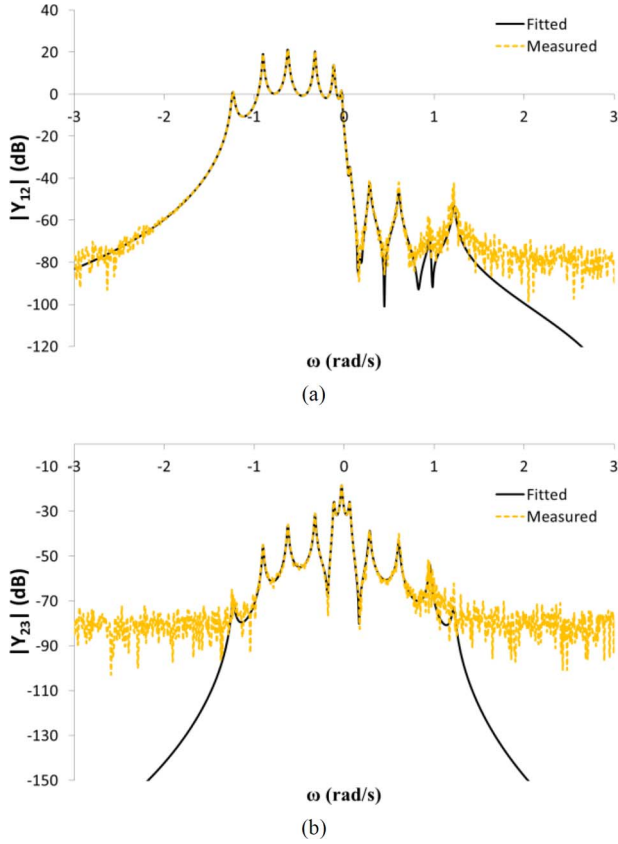


Fig. 5. (a) Measured and fitted Y_{12} with the MVF approach. (b) Measured and fitted Y_{23} with the MVF approach.

IV. SYNTHESIS OF THE TRANSVERSAL COUPLING MATRIX

The poles a_k and the residues r_{pq}^k can be obtained once the MVF procedure has converged and the rational functions are transformed to the form of

$$Y_{pq} = K_{pq} + \sum_{k=1}^N \frac{r_{pq}^k}{s - a_k}. \quad (13)$$

Comparing (13) with (2), it can be seen that the relationship between the poles and residues of the Y -parameter rational functions and the elements in the transversal coupling matrix is

$$\begin{aligned} M_{P1,k}^2 &= r_{11}^k \\ M_{P1,k}M_{P2,k} &= r_{12}^k \\ M_{P1,k}M_{P3,k} &= r_{13}^k \\ M_{P2,k}^2 &= r_{22}^k \\ M_{P2,k}M_{P3,k} &= r_{23}^k \\ M_{P3,k}^2 &= r_{33}^k \\ M_{k,k} &= 1j^*a_k, \quad k = 1, 2, \dots, N. \end{aligned} \quad (14)$$

From (14), it can be seen that in order to synthesize a transversal coupling matrix, the residues should satisfy the compactness condition

$$\begin{aligned} r_{12}^k r_{12}^k &= r_{11}^k r_{22}^k \\ r_{13}^k r_{13}^k &= r_{11}^k r_{33}^k \\ r_{23}^k r_{23}^k &= r_{22}^k r_{33}^k, \quad k = 1, 2, \dots, N. \end{aligned} \quad (15)$$

Since no constraint is applied to the residues in the MVF procedure, (15) is not guaranteed to be satisfied. However, when applying the MVF formulation to measured data of the diplexer, it is observed that (15) is automatically satisfied with only very small errors. Therefore, a transversal coupling matrix can be synthesized with the following strategy:

for $k = 1$ to N

$$M_{k,k} = 1j^*a_k$$

if $|r_{11}^k| > |r_{22}^k|$ and $|r_{11}^k| > |r_{33}^k|$

$$M_{P1,k} = \sqrt{r_{11}^k}, M_{P2,k} = r_{12}^k / \sqrt{r_{11}^k}, M_{P3,k} = r_{13}^k / \sqrt{r_{11}^k}$$

elseif $|r_{22}^k| > |r_{11}^k|$ and $|r_{22}^k| > |r_{33}^k|$

$$M_{P2,k} = \sqrt{r_{22}^k}, M_{P1,k} = r_{12}^k / \sqrt{r_{22}^k}, M_{P3,k} = r_{23}^k / \sqrt{r_{22}^k}$$

elseif $|r_{33}^k| > |r_{11}^k|$ and $|r_{33}^k| > |r_{22}^k|$

$$M_{P3,k} = \sqrt{r_{33}^k}, M_{P1,k} = r_{13}^k / \sqrt{r_{33}^k}, M_{P2,k} = r_{23}^k / \sqrt{r_{33}^k}$$

end

$$M_{k,P1} = M_{P1,k}, M_{k,P2} = M_{P2,k}, M_{k,P3} = M_{P3,k},$$

end

$$M_{P1,P1} = K_{11}/1j, M_{P2,P2} = K_{22}/1j, M_{P3,P3} = K_{33}/1j$$

where $1j$ stands for the imaginary unit j in a complex number, and $M_{x,y}$ denotes the element in the row of node x and column of node y in the coupling matrix \mathbf{M} .

For example, the poles and residues obtained for one of the tuning states of the testing diplexer are listed in Table I. The synthesized transversal coupling matrix using the proposed strategy above is given in Table II. The responses of the synthesized coupling matrix are superimposed to the raw measured data for comparison in Fig. 6. It can be seen that the responses of the extracted transversal coupling matrix agree well with the measured data up to -80 dB.

V. TRANSFORMATION OF THREE-PORT COUPLING MATRIX

The derivation of the transversal coupling matrix alone cannot help with the tuning of the diplexer because one-to-one correspondence between physical tuning elements and the coupling matrix elements is established only after the matrix is transformed to the right configuration. Many coupling matrix rotation recipes are available for coupled-resonator filters [18], and a general multi-port coupling matrix reconfiguration procedure is proposed in [19], where many coupling topologies are discussed. However, for the star-junction diplexers with resonant types of junctions discussed in this paper, a straightforward procedure exists and can be implemented in the diplexer circuit model extraction program.

A. General Procedure for Diplexers

The three-port coupling matrix of the diplexer can be reconfigured by matrix similarity transformation by following the same rules for filter transformations, i.e.,

$$[\mathbf{M}'] = [\mathbf{R}][\mathbf{M}][\mathbf{R}]^T \quad (16)$$

TABLE I
TABLE OF OBTAINED POLES AND RESIDUES BY MVF APPROACH FROM MEASURED DATA OF THE TESTING DIPLEXER

k	a_k	r_{1k}^k	r_{2k}^k	r_{3k}^k	r_{4k}^k	r_{5k}^k	r_{6k}^k
1	-0.012859 -1.24159i	0.511929 -0.012892i	0.0146850 +0.000389i	-0.000134 +5.70E-06i	0.000430 +0.000013i	-3.92E-06 -3.07E-08i	-0.000026 -0.000040i
2	-0.014466 +1.222349i	0.520280 +0.021701i	0.000031 -3.84E-07i	-0.034704 +0.000668i	-0.000020 +8.97E-06i	-3.20E-06 +5.18E-07i	0.002398 -0.000234i
3	-0.008776 +0.950428i	0.052779 -0.001669i	4.97E-06 +1.31E-07i	0.109793 +0.000138i	-3.21E-06 +5.17E-06i	0.000019 -1.57E-06i	0.226183 +0.007621i
4	-0.007348 -0.904463i	0.047768 +0.001087i	-0.066367 -0.000443i	-0.000031 +5.05E-07i	0.092061 -0.001089i	0.000040 -1.39E-07i	-0.000023 -0.000016i
5	-0.007862 -0.628855i	0.104160 -0.000069i	0.098399 +0.000035i	-0.000135 +3.80E-06i	0.092859 +0.000169i	-0.000126 -6.60E-08i	-0.000028 -0.000010i
6	-0.009633 +0.606357i	0.127717 +0.001289i	0.000049 +8.94E-07i	-0.154743 -0.001841i	-0.000010 +7.31E-07i	-0.000068 +1.96E-06i	0.188073 +0.002431i
7	-0.009049 +0.280957i	0.093699 +0.002180i	0.000071 +9.87E-07i	0.127928 +0.002146i	0.127928 +3.19E-06i	-5.69E-06 +2.66E-06i	0.000108 +0.002253i
8	-0.007042 -0.326218i	0.088139 -0.000831i	-0.073625 +0.000309i	-0.000237 +3.90E-06i	0.061742 -0.000027i	0.000200 -2.42E-06i	-0.000030 +4.78E-06i
9	-0.0086150 +0.059524i	0.018837 +0.001678i	-0.000135 -4.00E-06i	-0.064955 -0.001797i	-5.90E-06 -0.000003i	0.000454 -0.000021i	0.222240 -0.006989i
10	-0.008059 +0.029940i	0.166423 +0.001559i	-0.009705 +0.000520i	0.017057 +0.000681i	0.000559 -0.000065i	-0.000988 +0.000023i	0.001703 +0.000209i
11	-0.006742 -0.117618i	0.015495 -0.001124i	0.036592 -0.000808i	0.000160 -8.74E-06i	0.0860988 +0.0022677i	0.000368 -2.77E-06i	-0.000023 +0.000028i

$K_{11} = 0.018102 - 0.001988i$, $K_{22} = 0.008361 - 0.000238i$, $K_{33} = 0.010579 + 0.002046i$

TABLE II
SYNTHESIZED THREE-PORT TRANSVERSAL COUPLING MATRIX CORRESPONDING USING THE MVF FORMULATION

	P1	P2	P3	1	2	3	4	5	6	7	8	9	10	11
P1	-0.0020 -0.0181i	0	0	0.7155 -0.0090i	0.7215 +0.0150i	0.2304 -0.0036i	0.2186 +0.0026i	0.3228 -0.0001i	0.3572 +0.0019i	0.3062 +0.0034i	0.2968 -0.0014i	0.1376 +0.0060i	0.4080 +0.0019i	0.1246 -0.0044i
P2	0	-0.0002 -0.0084i	0	0.0205 +0.0008i	0	0	-0.3034 +0.0018i	0.3048 +0.0003i	0.0001	0.0002	-0.2483	-0.0010	-0.0238 +0.0014i	0.2935 +0.0039i
P3	0	0	0.0020 -0.0106i	-0.0002	-0.0481 +0.0019i	0.4757 +0.008i	-0.0001	-0.0004	-0.4336 -0.0028i	0.4178 +0.0026i	-0.0008	-0.4715 +0.0074i	0.0418 +0.0015i	0.0013
1	0.7155 -0.0090i	0.0205 +0.0008i	-0.0002	1.2416 -0.0129i	0	0	0	0	0	0	0	0	0	0
2	0.7215 +0.0150i	0	-0.0481 +0.0019i	0	-1.2223 -0.0145i	0	0	0	0	0	0	0	0	0
3	0.2304 -0.0036i	0	0.4757 +0.0080i	0	0	-0.9504 -0.0088i	0	0	0	0	0	0	0	0
4	0.2186 +0.0026i	-0.3034 +0.0018i	-0.0001	0	0	0	0.9045 -0.0073i	0	0	0	0	0	0	0
5	0.3228 -0.0001i	0.3048 +0.0003i	-0.0004	0	0	0	0	0.6289 -0.0079i	0	0	0	0	0	0
6	0.3572 +0.0019i	0.0001	-0.4336 -0.0028i	0	0	0	0	0	-0.6064 -0.0096i	0	0	0	0	0
7	0.3062 +0.0034i	0.0002	0.4178 +0.0026i	0	0	0	0	0	0	-0.2810 -0.0090i	0	0	0	0
8	0.2968 -0.0014i	-0.2483	-0.0008	0	0	0	0	0	0	0	0.3262 -0.0070i	0	0	0
9	0.1376 +0.0060i	-0.0010	-0.4715 +0.0074i	0	0	0	0	0	0	0	0	-0.0595 -0.0086i	0	0
10	0.4080 +0.0019i	-0.0238 +0.0014i	0.0418 +0.0015i	0	0	0	0	0	0	0	0	0	0.0299 -0.0081i	0
11	0.1246 -0.0044i	0.2935 +0.0039i	0.0013	0	0	0	0	0	0	0	0	0	0	0.1176 -0.0067i

where \mathbf{R} is an orthogonal rotation matrix, which can be specified by a pivot $[i, j]$ and a rotation angle θ . Since the port nodes are arranged as the first three nodes in the matrix, the pivot index cannot enter the first three rows and columns, i.e., $i, j \neq 1, 2, 3$. By the same token with filter cases, the transformation (16) can change the coupling topology of the network while reserving the reflection and transfer characteristics of the network. Note that if the coupling matrix represents a lossy network, both \mathbf{M} and \mathbf{R} in (16) are complex matrices.

The transformation procedure to reconfigure the three-port transversal coupling matrix to the desired coupling topology

for star-junction diplexers with resonant types of junctions can be divided into the following three steps.

- Step 1) Eliminate the non-existing I/O couplings. This procedure will create non-zero cross couplings between every two resonators.
- Step 2) Eliminate the non-existing cross couplings between the two channel filters. After this step, the three-port coupling matrix will be transformed into a block form, in which the coupling matrices for the two channel filters are separated into different blocks.
- Step 3) Transform the block matrix for each channel filter to the desired topology.

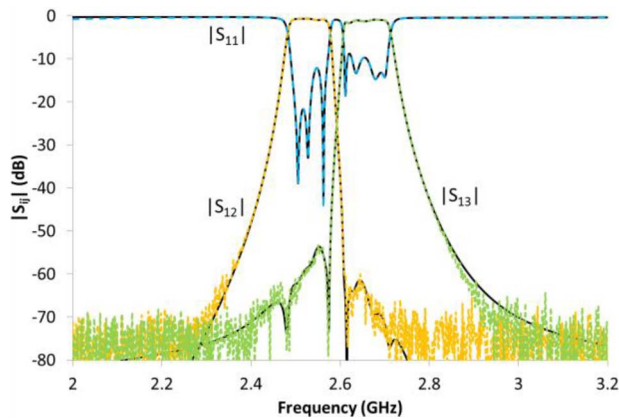


Fig. 6. Comparison of the measured and fitted S_{11} , S_{12} , and S_{13} data with the model extracted by MVF formulation. Dashed color lines are measured data. Black solid lines are the response given by the extracted three-port transversal coupling matrix with the MVF technique.

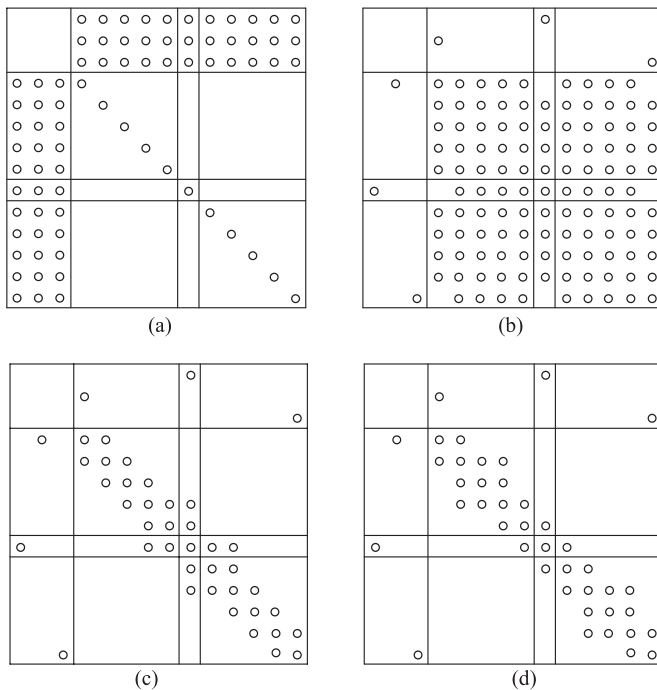


Fig. 7. (a) Transversal coupling matrix. (b) Matrix after I/O coupling are annihilated. (c) Matrix after the couplings between the two channel filters are annihilated to the best effort. (d) Final target topology.

The last step allows the utilization of those well-established filter transformation strategies in [18] since the two channel filters can be reconfigured individually. Thus the general procedure can be applied to those diplexers that are composed of high-degree channel filters and with many TZs connected by a common resonator junction.

B. Specific Example

In this paper, a customized recipe is introduced to transform the three-port transversal coupling matrix to the desired coupling topology for the testing diplexer shown in Fig. 3(b) by following the three steps in the general procedure.

TABLE III
ROTATION SEQUENCE TO RECONFIGURE THE COUPLING MATRIX

Rotation Sequence	Elements to be annihilated	Pivot $[i, j]$	Rotation Sequence	Elements to be annihilated	Pivot $[i, j]$
1	[P1, 1]	[1, 6]	31	[1, 7]	[7, 5]
2	[P1, 2]	[2, 6]	32	[1, 5]	[5, 4]
3	[P1, 3]	[3, 6]	33	[1, 4]	[4, 3]
4	[P1, 4]	[4, 6]	34	[1, 3]	[3, 2]
5	[P1, 5]	[5, 6]	35	[11, 3]	[3, 4]
6	[P1, 7]	[7, 6]	36	[11, 4]	[4, 5]
7	[P1, 8]	[8, 6]	37	[11, 5]	[5, 7]
8	[P1, 9]	[9, 6]	38	[11, 7]	[7, 8]
9	[P1, 10]	[10, 6]	39	[11, 8]	[8, 9]
10	[P1, 11]	[11, 6]	40	[11, 9]	[9, 10]
11	[P2, 2]	[2, 1]	41	[2, 9]	[9, 8]
12	[P2, 3]	[3, 1]	42	[2, 8]	[8, 7]
13	[P2, 4]	[4, 1]	43	[2, 7]	[7, 5]
14	[P2, 5]	[5, 1]	44	[2, 5]	[5, 4]
15	[P2, 7]	[7, 1]	45	[2, 4]	[4, 3]
16	[P2, 8]	[8, 1]	46	[10, 4]	[4, 5]
17	[P2, 9]	[9, 1]	47	[10, 5]	[5, 7]
18	[P2, 10]	[10, 1]	48	[10, 7]	[7, 8]
19	[P2, 11]	[11, 1]	49	[10, 8]	[8, 9]
20	[P3, 2]	[2, 11]	50	[3, 8]	[8, 7]
21	[P3, 3]	[3, 11]	51	[3, 7]	[7, 5]
22	[P3, 4]	[4, 11]	52	[3, 5]	[5, 4]
23	[P3, 5]	[5, 11]	53	[9, 5]	[5, 7]
24	[P3, 7]	[7, 11]	54	[9, 7]	[7, 8]
25	[P3, 8]	[8, 11]	55	[4, 7]	[7, 5]
26	[P3, 9]	[9, 11]	56	[6, 8]	[8, 7]
27	[P3, 10]	[10, 11]	57	[7, 9]	[9, 8]
28	[1, 10]	[10, 9]	58	[6, 4]	[4, 5]
29	[1, 9]	[9, 8]	59	[5, 3]	[3, 4]
30	[1, 8]	[8, 7]			

The matrix transformation procedure is depicted in Fig. 7(a)–(d), where the hollow circles represent expected non-zero entries at each stage. The first three rows/columns of the coupling matrix correspond to P1–P3 in Fig. 3(b) and the remaining 11 rows/columns correspond to resonators No. 1–11. Resonators No. 1–5 constitute the lower band channel filter and resonators No. 7–11 constitute the upper band channel filter. Resonator No. 6 is the common resonant node. The coupling matrices in Fig. 7 are partitioned according to the role that each row/column plays for a clear demonstration of the coupling matrix reconfiguration procedure. Fig. 7(a) is the three-port transversal coupling matrix. In the first step, non-existing I/O couplings are annihilated. The resultant matrix configuration is shown in Fig. 7(b). In the second stage, the cross-couplings between the two channel filters are annihilated as many as possible. This leaves the TZ of each channel filter with a trisection connected to the common resonator. In the last stage, the trisections are “pulled” to the right positions. The non-zero entries in the coupling matrix in Fig. 7(d) have a one-to-one relationship with the coupling topology of Fig. 3(b). The details of the rotation sequence are provided in Table III, where the 1 ~ 27 steps correspond to stage I, 28 ~ 55 steps correspond to stage II and the last four steps are in stage III. Once the first two stages are finished, the cross couplings will be separated into the two channel filters. Having had that, the reconfiguration of each channel filter can be done individually with well-established filter transformation recipes in [18].

TABLE IV
FINAL COUPLING MATRIX

	P1	P2	P3	1	2	3	4	5	6	7	8	9	10	11
P1	-0.0020 -0.0181i	0	0	0	0	0	0	0	1.3219 +0.0049i	0	0	0	0	0
P2	0	-0.0002 -0.0084i	0	0.5777 +0.0012i	0	0	0	0	0	0	0	0	0	0
P3	0	0	0.0020 -0.0106i	0	0	0	0	0	0	0	0	0	0	0.9028 +0.0029i
1	0	0.5777 +0.0012i	0	0.5168 -0.0110i	0.3064 +0.0001i	0	0	0	0	0	0	0	0	0
2	0	0	0	0.3064 +0.0001i	0.5067 -0.0052i	0.2056 +0.0011i	0.0882 -0.0028i	0	0	0	0	0	0	0
3	0	0	0	0	0.2056 +0.0011i	0.3941 +0.0009i	0.2015 +0.0009i	0	0.0152 +0.0003i	0	0	0	0	0
4	0	0	0	0	0.0882 -0.0028i	0.2015 +0.0009i	0.5685 -0.0041i	0.2560 +0.0013i	0.0065 -0.0001i	-0.0010 +0.0060i	0	0	0	0
5	0	0	0	0	0	0	0.2560 +0.0013i	0.6032 -0.0089i	0.7055 +0.0086i	-0.0001 -0.0079i	0.0058 -0.0051i	0	0	0
6	1.3219 +0.0049i	0	0	0	0	0.0152 +0.0003i	0.0065 -0.0001i	0.7055 +0.0086i	-0.0066 -0.0353i	0.7135 -0.0079i	0	0	0	0
7	0	0	0	0	0	0	-0.0010 +0.0060i	-0.0001 -0.0079i	0.7135 -0.0079i	-0.5470 -0.0102i	0.2762 -0.0009i	0	0	0
8	0	0	0	0	0	0	0	0.0058 -0.0051i	0	0.2762 -0.0009i	-0.5318 -0.0043i	0.2120 -0.0008i	-0.0915 -0.0023i	0
9	0	0	0	0	0	0	0	0	0	0	0.2120 -0.0008i	-0.3514 -0.0006i	0.2312 -0.0010i	0
10	0	0	0	0	0	0	0	0	0	0	-0.0915 -0.0023i	0.2312 -0.0010i	-0.5398 -0.0049i	0.3521 -0.0002i
11	0	0	0.9028 +0.0029i	0	0	0	0	0	0	0	0	0	0.3521 -0.0002i	-0.4835 -0.0166i

The distribution of the non-zero entries in Fig. 7(a)–(d) is verified by ideal cases with the specific coupling topology. However, when the rotation strategy is applied to the extracted coupling matrix, some stray couplings may be left in addition to the normal couplings. Starting from the obtained transversal coupling matrix in Table II and following the proposed matrix rotation sequence in Table III, one can obtain a coupling matrix as given in Table IV. It is seen that some of the non-zero entries shown in bold fonts do not correspond to any coupling element in Fig. 3(b). They are left over as lumped effects of all the spurious stray couplings in the diplexer. Normally their absolute values are smaller compared with those of normal couplings. It is also noticed that all the matrix elements present small imaginary parts, which count for the power dissipation of the resonant cavities as well as the coupling elements like the lossy filter coupling matrix [20].

The measured data of the testing diplexer are used to demonstrate the robustness and effectiveness of the proposed method. Since there is one-to-one correspondance between the entries in the coupling matrix and physical tuning elements, the extracted model provides a direct guidance on the tuning process. Four different tuning states are plotted in Fig. 8(a)–(d). In Fig. 8(a), the two channels overlap each other in the spectrum because some of the resonators are badly detuned. The passbands of the two channels become recognizable in Fig. 8(b) although the ports are still poorly matched. Fig. 8(c) corresponds to a state in the fine tuning stage, where the responses of the device are extremely sensitive to the depth of the tuning screws. Then very careful and subtle adjustments should be made. Fig. 8(d) shows the final well-tuned state where the common port reflection coefficient is lower than -20 dB within both passbands. The coupling coefficients corresponding to the four states are obtained by the MVF method and the proposed

TABLE V
EXTRACTED COUPLING VALUE CORRESPONDING TO THE FOUR STATES IN FIG. 8

	State 1	State 2	State 3	State 4
M_{11}	0.4202	0.4204	0.7065	0.6026
M_{22}	0.2633	0.6375	0.6284	0.6291
M_{33}	0.2354	0.2412	0.4606	0.4612
M_{44}	-0.1768	0.6066	0.6121	0.6151
M_{55}	0.3353	0.3342	0.7073	0.6343
M_{66}	-0.0406	-0.0452	-0.0516	0.1105
M_{77}	-0.0818	-0.2943	-0.5079	-0.5846
M_{88}	0.0000	-0.6067	-0.6100	-0.6121
M_{99}	-0.4508	-0.4479	-0.4455	-0.4478
$M_{10,10}$	-0.5786	-0.5810	-0.5811	-0.6163
$M_{11,11}$	0.5885	-0.5836	-0.5835	-0.6093
M_{12}	0.3747	0.3776	0.3709	0.3660
M_{23}	0.2563	0.2486	0.2388	0.2387
M_{34}	0.2672	0.2254	0.2343	0.2345
M_{45}	0.2841	0.3048	0.2914	0.2939
M_{56}	0.7906	0.7933	0.7928	0.7819
M_{67}	0.7541	0.7661	0.7883	0.7928
M_{78}	0.2881	0.2970	0.2951	0.2949
M_{89}	0.2265	0.2341	0.2331	0.2330
$M_{9,10}$	0.2365	0.2363	0.2358	0.2376
$M_{10,11}$	0.3301	0.3492	0.3492	0.3491
M_{24}	0.0818	0.0812	0.0838	0.0894
$M_{8,10}$	-0.0859	-0.0899	-0.0913	-0.0906
M_{36}^*	0.0108	0.0119	0.0122	0.0123
$M_{P1,6}$	1.3942	1.3919	1.3916	1.3844
$M_{P2,1}$	0.6924	0.6927	0.6880	0.6899
$M_{P3,11}$	0.6434	0.6483	0.6485	0.6488

* A large stray coupling left after the proposed coupling matrix reduction scheme.

coupling matrix reconfiguration strategy, and their real parts are listed in Table V. The responses given by the extracted coupling matrix are superimposed on the raw measured data in Fig. 8. Very good agreement is achieved for all tuning states.

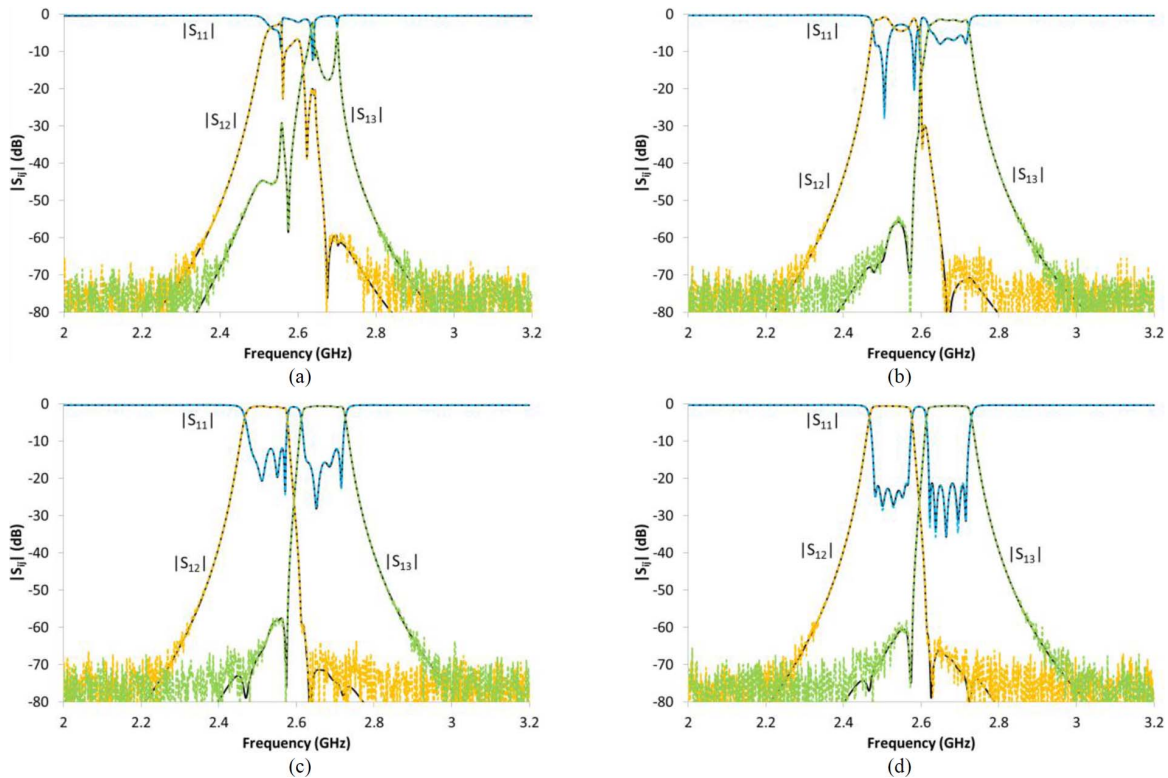


Fig. 8. Four different tuning states of the testing diplexer. Solid black lines are the response given by the extracted coupling matrix. Dashed lines are measured data.

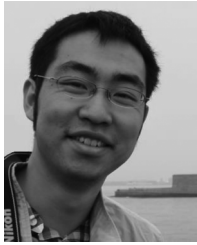
VI. CONCLUSION

In this paper, a practical circuit model extraction method for coupled-resonator diplexers with resonant types of junctions has been proposed for the first time. All the self-coupling and mutual coupling values of the diplexer can be determined together to reveal the current tuning state of the device. It utilizes the MVF to accurately determine the rational system functions from the noise-contaminated measurement data. A transversal coupling matrix of the coupled-resonator network can then be obtained. A three-port coupling matrix orthogonal transformation strategy has been proposed to transform the transversal coupling matrix to the desired matrix configuration corresponding to the physical realization. The MVF technique and the synthesis and reconfiguration of the three-port coupling matrix together form a complete scheme to extract the circuit model from the measured frequency-domain response of coupled-resonator diplexers with resonant types of junctions. A testing diplexer has been used and fine tuned with the help of the proposed method for illustration. The proposed method can be implemented in a robotic tuning system for smart manufacturing.

REFERENCES

- [1] M. E. Van Valkenburg, *Introduction to Modern Network Synthesis*. New York, NY, USA: Wiley, 1960.
- [2] T. Skaik, M. Lancaster, and F. Huang, "Synthesis of multiple output coupled resonator circuits using coupling matrix optimization," *IET Microw. Antennas Propag.*, vol. 5, no. 9, pp. 1081–1088, Jun. 2011.
- [3] S. Tamiasso and G. Macchiarella, "Synthesis of duplexers with the common port matched at all frequencies," *IEEE Trans. Microw. Theory Techn.*, vol. 62, no. 1, pp. 46–54, Jan. 2014.
- [4] L. Zhao, L. Yeung, and K.-L. Wu, "A coupled resonator decoupling network for two-element compact antenna arrays in mobile terminals," *IEEE Trans. Antennas Propag.*, vol. 62, no. 5, pp. 2767–2776, May 2014.
- [5] Q. Zhang, T. Guo, B. A. Khan, T. Kodera and C. Caloz, "Coupling matrix synthesis of nonreciprocal lossless two-port networks using gyrators and inverters," *IEEE Trans. Microw. Theory Techn.*, vol. 63, no. 9, pp. 2782–2792, Sep. 2015.
- [6] J. B. Ness, "A unified approach to the design, measurement, and tuning of coupled-resonator filters," *IEEE Trans. Microw. Theory Techn.*, vol. 46, no. 4, pp. 343–351, Apr. 1998.
- [7] P. Harscher, R. Vahldieck, and S. Amari, "Automated filter tuning using generalized low-pass prototype networks and gradient-based parameter extraction," *IEEE Trans. Microw. Theory Techn.*, vol. 49, no. 12, pp. 2532–2538, Dec. 2001.
- [8] G. Macchiarella and D. Traina, "A formulation of the Cauchy method suitable for the synthesis of lossless circuit models of microwave filters from lossy measurements," *IEEE Microw. Wireless Compon. Lett.*, vol. 16, no. 5, pp. 243–245, May 2006.
- [9] M. Meng and K.-L. Wu, "An analytical approach to computer-aided diagnosis and tuning of lossy microwave coupled resonator filters," *IEEE Trans. Microw. Theory Techn.*, vol. 57, no. 12, pp. 3188–3195, Dec. 2009.
- [10] G. Macchiarella, "Extraction of unloaded Q and coupling matrix from measurement on filters with large losses," *IEEE Microw. Wireless Compon. Lett.*, vol. 20, no. 6, pp. 307–309, Jun. 2010.
- [11] H. Hu and K.-L. Wu, "A generalized coupling matrix extraction technique for bandpass filters with uneven-Qs," *IEEE Trans. Microw. Theory Techn.*, vol. 62, no. 2, pp. 244–251, Feb. 2014.
- [12] D. Traina, G. Macchiarella, and T. K. Sarkar, "Robust formulations of the Cauchy method suitable for microwave duplexers modeling," *IEEE Trans. Microw. Theory Techn.*, vol. 55, no. 5, pp. 974–982, May 2007.
- [13] P. Zhao and K.-L. Wu, "Circuit model extraction for computer-aided tuning of a coupled-resonator diplexer," in *IEEE MTT-S Int. Microw. Symp. Dig.*, Phoenix, AZ, USA, May 2015.
- [14] A. Garcia-Lamperez and M. Salazar-Palma, "Analytical synthesis of coupling matrices for N-port networks with reactance compensation," in *Eur. Microw. Week Adv. N-Port Netw. Space Appl. Workshop*, Amsterdam, The Netherlands, Oct. 2012.
- [15] P. Zhao and K.-L. Wu, "An iterative and analytical approach to optimal synthesis of a multiplexer with a star-junction," *IEEE Trans. Microw. Theory Techn.*, vol. 62, no. 12, pp. 3362–3369, Dec. 2014.

- [16] B. Gustavsen and A. Semlyen, "Simulation of transmission line transients using vector fitting and modal decomposition," *IEEE Trans. Power Del.*, vol. 13, no. 2, pp. 605–614, Apr. 1998.
- [17] B. Gustavsen and A. Semlyen, "Rational approximation of frequency domain responses by vector fitting," *IEEE Trans. Power Delivery*, vol. 14, no. 3, pp. 1052–1061, Jul. 1999.
- [18] R. J. Cameron, C. M. Kudsia, and R. R. Mansour, *Microwave Filters for Communication Systems: Fundamentals, Design and Applications*. Hoboken, NJ, USA: Wiley, 2007.
- [19] G. Macchiarella and S. Tamiazzo, "Generation of canonical forms for multiport filtering networks," in *IEEE MTT-S Int. Microw. Symp. Dig.*, Tampa, FL, USA, Jun. 2014.
- [20] V. Mirafteb and M. Yu, "Generalized lossy microwave filter coupling matrix synthesis and design using mixed technologies," *IEEE Trans. Microw. Theory Techn.*, vol. 56, no. 12, pp. 3016–3027, Dec. 2008.



Ping Zhao (S'14) received the B.Sc. degree from Nanjing University, Nanjing, China, in 2012, and is currently working toward the Ph.D. degree at The Chinese University of Hong Kong, Shatin, Hong Kong.

His research is focused on synthesis and computer-aided tuning (CAT) algorithms for multiport microwave coupled-resonator networks, including diplexers, multiplexers, and coupled-resonator decoupling networks with applications in cellular base stations and satellites.

Mr. Zhao was the recipient of the Honorable Mention in the 2014 IEEE Microwave Theory and Techniques Society (IEEE MTT-S) International Microwave Symposium (IMS) Student Paper Competition. He was also the recipient of the Best Student Paper Award of the 2014 IEEE HK AP/MTT Postgraduate Conference.



Ke-Li Wu (M'90–SM'96–F'11) received the B.S. and M.Eng. degrees from the Nanjing University of Science and Technology, Nanjing, China, in 1982 and 1985, respectively, and the Ph.D. degree from Laval University, Quebec, QC, Canada, in 1989.

From 1989 to 1993, he was with the Communications Research Laboratory, McMaster University, as a Research Engineer and a Group Manager. In March 1993, he joined the Corporate R&D Division, COM DEV International (the largest Canadian space equipment manufacturer), where he was a Principal Member of Technical Staff. Since October 1999, he has been with The Chinese University of Hong Kong, Shatin, Hong Kong, where he is currently a Professor and the Director of the Radiofrequency Radiation Research Laboratory (R3L). He has authored or coauthored numerous publications in the areas of electromagnetic (EM) modeling and microwave passive components, microwave filters, and antenna engineering. His current research interests include partial element equivalent circuit (PEEC) and derived physically expressive circuit (DPEC) EM modeling of high-speed circuits, RF and microwave passive circuits and systems, synthesis theory and practices of microwave filters, antennas for wireless terminals, low-temperature co-fired ceramic (LTCC)-based multichip modules (MCMs), and RF identification (RFID) technologies.

Prof. Wu is a Member of the IEEE MTT-8 Subcommittee (Filters and Passive Components). He also serves as a Technical Program Committee (TPC) Member for many prestigious international conferences including the IEEE Microwave Theory and Techniques Society (IEEE MTT-S) International Microwave Symposium (IMS). He was an Associate Editor for the IEEE TRANSACTIONS ON MICROWAVE THEORY AND TECHNIQUES from 2006 to 2009. He was the recipient of the 1998 COM DEV Achievement Award for the development of exact EM design software of microwave filters and multiplexers and the Asia-Pacific Microwave Conference Prize in 2008 and 2012, respectively.